Analytica Chimica Acta xxx (2018) 1–9

Contents lists available at ScienceDirect

Analytica Chimica Acta

journal homepage: www.elsevier.com/locate/aca

A novel DNA sensor based on C_{60}NPs-PAMAM-PtPNPs to detect VKORC1 gene for guiding rational clinical therapy with warfarin

Yongxian Wan [a], Lili Xu [b], Naiqiang Zhuo [a], Xiaobo Lu [a, *]

[a] Department of Orthopedics, Affiliated Hospital of Southwest Medical University, Luzhou, China
[b] Department of Rehabilitation Medicine, Affiliated Hospital of Southwest Medical University, Luzhou, China

HIGHLIGHTS

- VKORC1 was detected by the DNA biosensor for the first time.
- This strategy demonstrates a new avenue for guiding rational clinical therapy with Warfarin.
- To improve the sensitivity, biotinylated tetrahedral DNA was introduced during the fabrication of the biosensor.

GRAPHICAL ABSTRACT

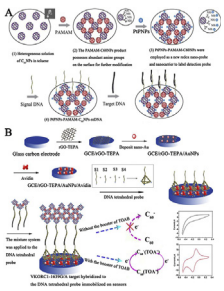

ARTICLE INFO

Article history:
Received 24 September 2017
Received in revised form
24 December 2017
Accepted 10 January 2018
Available online xxx

Keywords:
C_{60}
Tetrahedral DNA
Vitamin K epoxide reductase complex subunit 1
Target therapy

ABSTRACT

Reports have indicated that warfarin is the most widely prescribed anticoagulant. However, traditionally prescribed doses for each patient may be too low or too high. The therapeutic effect is often hindered by a lack of evidence-based medical information. Herein, our aim is to provide this information. To accomplish this challenge, we report the development of a novel assay based on biotinylated tetrahedral DNA as a capture probe and fullerene (C_{60})-based nanomaterial as a redox probe using an ultrasensitivity assay with the Vitamin K epoxide reductase complex, subunit 1 (VKORC1). Platinum porous nanoparticles (PtPNPs) were modified on amino-terminated polyamidoamine (PAMAM)-functionalized C_{60} nanoparticles (C_{60}NPs). The resultant C_{60}NPs-PAMAM-PtPNPs were used as a redox probe. In this design, C_{60} exhibited excellent redox activity that was triggered by tetraoctylammonium bromide (TOAB). To improve the immobilization of the tetrahedral DNA capture probe, avidin was introduced during the fabrication of the biosensor because it can provide more active sites for the immobilization capture probe. The free-standing probe on top of the tetrahedral DNA served as a receptor to hybridize with target DNA directly. Different pulse voltammetry (DPV) was applied to record the electrochemical signals, which increased linearly with the target DNA. Under optimal conditions, the prepared biosensor showed a wide linear relationship, from 1 pM to 10 nM, with detection limits of 0.33 pM. This strategy demonstrates a new avenue for the determination of tumour-related mutated nucleotides in biosamples.

1. Introduction

Vitamin K epoxide reductase complex, subunit 1 (VKORC1) -1639G/A genotype, is one of the strongest genetic factors that is used to determine warfarin effects in preventing thrombosis,

* Corresponding author. Department of Orthopedics, PROOF Affiliated Hospital of Southwest Medical University, No. 20 of Taiping Street in the Jiangyang district, Luzou City, Sichuan Province, 646000, China.
E-mail address: wyx20170820@163.com (X. Lu).

https://doi.org/10.1016/j.aca.2018.01.028
0003-2670/

thromboembolism, and many other disorders [1,2]. The mutation led to a significantly lower daily dose of warfarin [3]. Warfarin is characterized by its narrow therapeutic index, wide interpatient variability of pharmacokinetic parameters and high toxicity [4,5]. It is crucial to prescreen patients for their genotypes before prescribing this drug to facilitate faster personalized therapy and minimize the risk for adverse reactions [6]. Herein, we report the development of a novel and sensitive electrochemical bioassay method that is applicable to this genotype; the possibility of using this method clinically was also examined.

To achieve high detection capabilities, the selection of the capture probe is a crucial feature for nucleic acid hybridization [7,8]. Alternative probes to classic single-stranded DNA (ssDNA) are under development, such as hairpin DNA [9], locked nucleic acid and tetrahedral DNA [10,11]. The sensitivity of biological sensors is often limited by low efficiency of heterogeneous biological reactions. Tetrahedral DNA has become a popular research topic in this field. Owing to the tetrahedral nanostructure not only proves structural stability and mechanical rigidity [7,12], but also ensures that the capture probes are oriented properly and have a controlled density. In addition, it well controlled spacing and orientation of DNA probes and greatly improved accessibility for bimolecular recognition compared with the traditional DNA sensor [13]. For advancing the tetrahedral, we used biotin replace −SH to modify three vertices of tetrahedral DNA. As a result, the sensitivity of biosensor is enhanced by controlling the biomolecule-confined surface and by increasing molecular recognition at the biosensor interface [9,14]. In recent years, although promising research has produced biosensors using a tetrahedral DNA probe to detect mutated nucleotides in biosamples [15,16]. To the best of our knowledge, an advanced tetrahedral DNA probe has not been used to identify the VKORC1 genotype. Thus, our goal in this work was to utilize the advantages of tetrahedral DNA to detect of VKORC1 -1639G/A. For amplifing the detection signal, avidin was introduced during biosensor fabrication. Because it can provide more active sites for the immobilization tetrahedral DNA probe, Leading to the specific recognition between avidin and biotin at three vertices of the tetrahedral [17–20]. In order to immobilization more avidin, reduced graphene oxide–tetraethylene pentamine (rGO–TEPA) and gold nanoparticles (AuNPs) were integrated. Based on rGO–TEPA not only keeps the original property of rGO but also promotes water solubility [21]. At the same time, AuNPs exhibited unique properties such as excellent conductivity, good biocompatibility and large surface areas.

For the development of an electrochemical bioassay, signal amplification is important to improve the sensitivity of a DNA biosensor. However, nucleotides are not intrinsically able to act as redox partners in a bioassay reaction. Therefore, the effective immobilization of a redox molecule is a key step in the fabrication of a sandwich-type DNA biosensor, which determines its linear range and detection limit [22]. Very recently, nanomaterial has been used as a redox probe because it is able to efficiently overcome the leakage of redox molecules and enhances the amount of immobilized biomolecules as nanocarriers. Fullerene (C_{60}), which has gained importance in materials science, provides a large surface area and good biocompatibility, as well as excellent conductivity [23–25]. Most importantly, C_{60} has a strong electron-accepting capacity and the ability to form corresponding anionic species; this makes it an ideal redox molecule for the construction of a sandwich-type biosensor [22]. Amino-terminated polyamidoamine (PAMAM) which is a hyper-branched and three-dimensional structure with good structural homogeneity and high density of surface active groups, was decorated C_{60} to improve its hydrophilicity and possesses abundant amine groups on the surface for further modification [22]. In order to improve the sensitive, platinum porous nanoparticles (PtPNPs) were introduced, owing to its high porosity, large surface area per unit volume [26] and can offer interconnected channels, which contribute to accelerate electron transfer between the electrode surface and target molecules and further improved the sensitive of the biosensor [27]. Meanwhile, the nanoporous structure can remarkably address the drawbacks of a bulk metal as an electrode material. To our surprise, the use of C_{60}NPs-PAMAM-PtPNPs combined TOAB system as a redox probe for DNA bioassays has not been reported in the literature.

We designed a novel sandwich-type DNA biosensor to enable the detection of VKORC1 -1639G/A. Biotinylated tetrahedral DNA was used as a capture probe and C_{60}-based nanomaterial was used as a redox probe. Although, the mutation gene can be detect based on rGO-TEPA/AuNPs/avidin/tetrahedral DNA/BSA modified electrode. For improving the sensitive, the C_{60}NPs-PAMAM-PtPNPs was used. To prepare a hydrophilic C_{60}-based nanoprobe, C_{60} nanoparticles (C_{60}NPs) were prepared by the phase-transfer method and then functionalized with PAMAM. The obtained PAMAM-decorated C_{60}NPs (C_{60}NPs-PAMAM) have better hydrophilicity compared to that of C_{60}NPs; additionally, there are abundant amine groups available for further modification. After PtPNPs were absorbed on the surface of the PAMAM-C_{60}NPs, the resultant C_{60}NPs-PAMAM-PtPNPs was used as a signal amplifier with a transducer when analysing DNA hybridization events. After a sandwich-type bioreaction, the resultant biosensor was incubated with tetraoctylammonium bromide (TOAB) to trigger the inner redox activity of C_{60} [22]. The signals were detected by differential pulse voltammetry (DPV) in a 0.1 M phosphate buffered solution (PBS). Furthermore, the specificity was also investigated by detect single-base mismatch (mismatch-1, wild type), two-base mismatch (mismatch-2), three-base mismatch (mismatch-3) and non-complementary target (random) oligonucleotides. The results show that the biosensor can specific detect the mutation gene. The strategy reported here is a new method of determining tumour-related mutated nucleotides in biosamples, relying on carbon-based materials as the redox nano-probe.

2. Experimental

2.1. Materials and chemicals

Reduced graphene oxide – tetraethylene pentamin (rGO-TEPA) and Fullerene (C_{60}) were provided by Nanjing XFNANO Materials TECH Co., Ltd. (China). Tetraoctylammonium bromide (TOAB, 98%) was purchased from J&K Scientific. Tris-(2-carboxyethyl)-phosphine hydrochloride (TCEP), Gold (III) chloride trihydrate ($HAuCl_4 \cdot 3H_2O$), Chloroplatinic acid (H_2PtCl_6), Avidin, Tetraoctylammonium bromide and amino-terminated polyamidoamine dendrimer (G5.0 PAMAM) were obtained from Sigma-Aldrich (St. Louis, USA, www.Sigma-Aldrich.com). Bovine Serum Albumin (BSA), potassium ferricyanide ($K_3Fe(CN)_6$) and potassium ferrocyanide ($K_4Fe(CN)_6$) were purchased from Beijing Chemical Reagents Company (Beijing, China). Clinical serum samples were obtained from a local hospital and stored at 4 °C. The DNA oligonucleotides were synthesized and purified by Shanghai RuiDi Biological Technology Co., Ltd. with their sequences illustrated in Table S1.

The buffer solutions involved in this study were as follow: 1 × TE buffer (10 mM Trishydroxymethylaminomethane hydrochloride (Tris-HCl), and 1.0 mM ethylenediaminetetraacetic acid (EDTA), pH 8.0), which was used to dissolve all oligonucleotides. The other buffer solutions are listed in Table S2. All other reagents were of analytical reagent grade and used without further purification. Ultrapure water (>18.2 MΩ) obtained from a Millipore Mill-Q purification system was used throughout the experiment.

Please cite this article in press as: Y. Wan, et al., A novel DNA sensor based on C_{60}NPs-PAMAM-PtPNPs to detect VKORC1 gene for guiding rational clinical therapy with warfarin, Analytica Chimica Acta (2018), https://doi.org/10.1016/j.aca.2018.01.028

2.2. Construction of the electrochemical DNA biosensor

The apparatus, and preparation of C_{60}NPs-PAMAM, C_{60}NPs-PAMAM-PtPNPs and the C_{60}NPs-PAMAM-PtPNPs-ssDNA detection probe are described in detail in the Supporting Information (S1). The tetrahedral structured DNA probes were self-assembled by DNA hybridization between three biotinylated DNA nucleotide sequences and a longer DNA nucleotide sequence containing the complementary sequence of the target sequence through a change in temperature. The tetrahedral DNA structure was prepared as previously reported [11,15]. First, 2 μL of S1, S2, S3 and S4 were mixed with 42 μL of the TM buffer. Then, the resulting mixture was incubated at 95 °C for 5 min and cooled to 4 °C for 30 s to form a tetrahedral DNA structure. The successful formation of the tetrahedral DNA was illustrated by sodium dodecyl sulphate-polyacrylamide gel electrophoresis (SDS-PAGE) in Fig. 3B.

The fabrication procedure of the electrochemical DNA biosensor is illustrated in Scheme 1B. Prior to use, GCE was polished repeatedly using 0.3- and 0.05-μm alumina slurries followed by thorough rinsing with Milli-Q water. After successive sonication in baths of Milli-Q water, absolute alcohol and Milli-Q water again, the electrode was dried at room temperature. After that, 8 μL of rGO-TEPA (2 mg mL^{-1}) was cast onto the electrode surface and dried in the air. Subsequently, AuNPs were electrochemically deposited onto the rGO-TEPA-modified GCE surface under a constant potential of −0.2 V for 30 s in a 1% $HAuCl_4$ solution referring to the previous literature [28,29]. After washing with Milli-Q water, 10 μL of an avidin solution (100 ng mL^{-1}) was dropped onto the modified electrode surface through the strong effect of Au-NH_2 bonding to immobilize avidin. The electrode was kept at 4 °C for 16 h, as avidin can retain its bioactivity for a long period of time at this temperature. After the reaction, the electrodes were washed with Milli-Q water to remove loosely bound chemicals and dried in nitrogen. Then, 10 μL of a tetrahedral DNA capture probe solution (10 nM) in immobilization buffer was injected onto the GCE/rGO-TEPA/AuNPs surface and incubated at room temperature for 10 h. Through the specific recognition between avidin and biotin, the biotinylated DNA tetrahedral probe was immobilized on the electrode surface for hybridization with target DNA. Next, the electrodes containing the DNA tetrahedral probe were rinsed with washing-buffer to eradicate nonspecifically absorbed probes. Finally, the modified immunosensor was incubated in a 1 wt% BSA solution for 1 h at 37 °C to eliminate nonspecific binding sites between the analyte and the electrode.

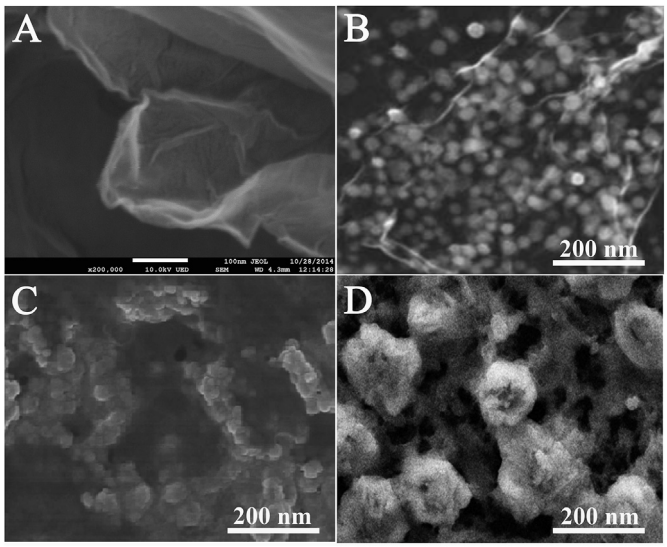

Fig. 1. FE-SEM images of (A) rGO-TEPA, (B) rGO-TEPA/AuNPs, (C) rGO-TEPA/AuNPs/avidin, and (D) rGO-TEPA/AuNPs/avidin/tetrahedral DNA.

2.3. Electrochemical measurements

Target DNA solutions with different concentrations were mixed with 100 nM C_{60}NPs-PAMAM-PtPNPs-ssDNA detection probe in a hybridization-buffer; then, the mixture was incubated at 37 °C for 1 h so that the target DNA could efficiently hybridize with the DNA tetrahedral capture probe. Then, the electrodes containing the DNA tetrahedral capture probe were washed with washing-buffer and dried in nitrogen. Afterwards, 8 μL of the above target solution was incubated with the decorated electrode for 1 h at 37 °C for hybridization. After the reaction, the electrodes were washed with washing-buffer to remove loosely bound adsorption molecules and dried in nitrogen. Subsequently, 10 μL of a TOAB toluene (10 mM) solution was cast on the above electrode for 10 min to trigger the inner redox activity of C_{60}. Finally, the electrochemical measurement with DPV was performed from -0.8 to 0.5 V (vs. SCE) in working buffer to record the electrochemical responses. The electrochemical responses were directly proportional to the concentrations of target DNA.

3. Results and discussion

3.1. Characteristics of the modified electrodes

The stepwise DNA biosensor fabrication processes were investigated by FE-SEM. From the FE-SEM image of rGO-TEPA, a wrinkled paper-like structure was observed (Fig. 1A). As shown from the FE-SEM image of the rGO-TEPA/AuNPs composite (Fig. 1B), AuNPs were clearly covered on the surface of rGO-TEPA, which further increased the surface area of rGO-TEPA. Compared with the FE-SEM image of the resulting rGO-TEPA/AuNPs/avidin composite (Fig. 1C), proteins are trapped on the surface of the rGO-TEPA/AuNPs, and a blurry surface image was observed, distinct from that shown in Fig. 1B. This result is indicative of successful avidin bonding on the surface of the rGO-TEPA/AuNPs. After the biotinylated DNA tetrahedral probe was conveniently immobilized on the rGO-TEPA/AuNPs/avidin surface, the FE-SEM image revealed island-like array shape with highly functional density and regular distribution (Fig. 1D). This shape is distinct from that shown in Fig. 1C, indicating that the DNA tetrahedral probe was successfully introduced via specific recognition between avidin and biotin.

To further confirm the successful modification of the DNA biosensor, the results were monitored by AFM. Fig. S1A shows the morphology of the rGO-TEPA surface, which has a roughness of 5.489 nm. After the electrodeposition of AuNPs on the rGO-TEPA surface, the roughness was increased to 365.4 nm (Fig. S1B), indicating that the AuNPs sufficiently increased the surface area of the electrode. As seen in Fig. 1SC, the roughness of the electrode decreased to 240.5 nm after the above-modified electrode was incubated with 100 nM avidin. This suggests that avidin molecules successfully bonded to the surface of the rGO-TEPA/AuNPs [30].

3.2. Characterization of the detection probes

SEM was used to demonstrate the successful synthesis of C_{60}NPs-PAMAM-PtPNPs. A typical nanoscale polygon or sphere shown in Fig. 2A. After the C_{60}NPs reacted with PAMAM, a textile structure was observed wrapped on the sphere surface. The refraction of C_{60}NPs-PAMAM was different from that of the C_{60}NPs, as shown in Fig. 2B. Typical SEM and TEM images of PtPNPs are shown in Fig. 2C and D. It was observed that the PtPNPs had a

Please cite this article in press as: Y. Wan, et al., A novel DNA sensor based on C_{60}NPs-PAMAM-PtPNPs to detect VKORC1 gene for guiding rational clinical therapy with warfarin, Analytica Chimica Acta (2018), https://doi.org/10.1016/j.aca.2018.01.028

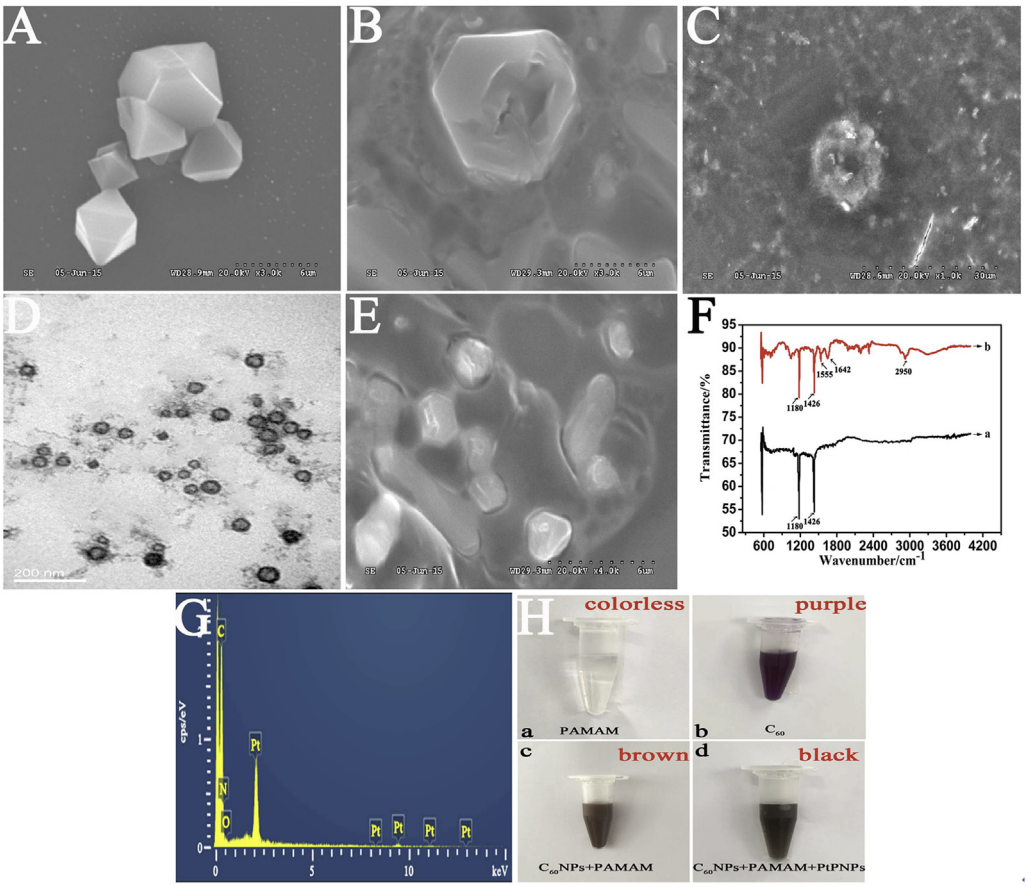

Fig. 2. SEM image of (A) C_{60}NPs, (B) C_{60}NPs-PAMAM, (C) PtPNPs and (E) C_{60}NPs-PAMAM-PtPNPs; (D) TEM image of PtPNPs; (F) FT-IR spectra of (a) C_{60}NPs and (b) C_{60}NPs-PAMAM; (G) EDS of C_{60}NPs-PAMAM-PtPNPs; (H) The colour changes during the preparation of the C_{60}NPs-PAMAM-PtPNPs. (For interpretation of the references to colour in this figure legend, the reader is referred to the Web version of this article.)

porous, spherical morphology and a rough surface. Fig. 2E shows typical SEM images of the C_{60}NPs-PAMAM-PtPNPs hybrids. The PtPNPs are trapped on the surface of the C_{60}NPs-PAMAM hybrids, indicating successful fabrication of C_{60}NPs-PAMAM-PtPNPs hybrids. In addition, the C_{60}NPs-PAMAM interaction was characterized by Fourier transform-infrared (FT-IR) spectrum. As shown in Fig. 2F, it is noted that the FT-IR spectrum of C_{60}NPs (curve a) and C_{60}NPs-PAMAM (curve b) both revealed C_{60}NPs absorption features at about 1180 cm^{-1} and 1426 cm^{-1}. The distinct band at 1180 cm^{-1} was attributed to C-H in-plane bending vibrations and the band at 1426 cm^{-1} was assigned to C=C vibrations [31]. Compared with curve a, in the C_{60}NPs-PAMAM spectra (curve b), spectral shifting was observed for the PAMAM C-N stretching the band at 1642^{-1} coupled with N-H bending at 1555 cm^{-1}, and the bands at 2950 cm^{-1} are contributed by CH_2 bending vibration, which corresponded to PAMAM [32–35]. The presence of all these absorption waves supports a successful synthesis of C_{60}NPs-PAMAM. In order to further prove the formation of C_{60}NPs-PAMAM-PtPNPs, EDS characterization was employed to analyse the detailed composition of the C_{60}NPs-PAMAM-PtPNPs. As shown in Fig. 2G, several intense peaks of Pt were observed, suggesting that the C_{60}NPs-PAMAM-PtPNPs hybrids had been successfully synthesized. The colour changes after each step was shown in Fig. 2H, which also identify the successful synthesise of C_{60}NPs-PAMAM-PtPNPs.

To assess the conjugation of the ssDNA detection probe to the C_{60}NPs-PAMAM-PtPNPs hybrids, UV absorption spectra were employed. As shown in Fig. 3A, it can be seen that the characteristic absorbance of ssDNA appeared at 260 nm (curve b) [36,37]. Meanwhile, compared to the absorption spectrum of the C_{60}NPs-PAMAM-PtPNPs (curve a), there is also an obvious absorption at 260 nm for the C_{60}NPs-PAMAM-PtPNPs-ssDNA detection probe (curve c), which suggests that the ssDNA detection probe had conjugated to the C_{60}NPs-PAMAM-PtPNPs hybrids. Based on the above results, we confirmed that the C_{60}NPs-PAMAM-PtPNPs-ssDNA detection probe was successfully prepared.

SDS-PAGE confirmed the successful assembly of a DNA tetrahedral, C_{60}NPs-PAMAM-PtPNPs-ssDNA detection probe hybridized with target DNA and the successful formation of the sandwich-type DNA biosensor. As shown in Fig. 3B, the ssDNA and two or three strands of DNA combination molecules moved quickly in lane a to p due to their low molecular weight. As expected, the DNA tetrahedral probe showed the lowest mobility in lane q, which is similar to previous reports [15]. The results provide evidence for the successful formation of the DNA tetrahedral probe. Analogously, the hybrid of C_{60}NPs-PAMAM-PtPNPs-ssDNA and target DNA (lane 3) was found to move more slowly than C_{60}NPs-PAMAM-PtPNPs-ssDNA (lane 1) and target DNA (lane 2), as shown in Fig. 3C. These results are in accordance with previously reported work [16]. The results prove that C_{60}NPs-PAMAM-PtPNPs-ssDNA successfully hybridized with target DNA. Furthermore, the successful formation of the sandwich-type DNA biosensor was confirmed. Fig. 3D shows that the hybrids of C_{60}NPs-PAMAM-PtPNPs-ssDNA, target DNA and tetrahedral DNA (lane 3) moved more slowly compared with C_{60}NPs-PAMAM-PtPNPs-ssDNA (lane 1) and tetrahedral DNA (lane 2), which could be attributed to the successful formation of a sandwich-type DNA biosensor.

Please cite this article in press as: Y. Wan, et al., A novel DNA sensor based on C_{60}NPs-PAMAM-PtPNPs to detect VKORC1 gene for guiding rational clinical therapy with warfarin, Analytica Chimica Acta (2018), https://doi.org/10.1016/j.aca.2018.01.028

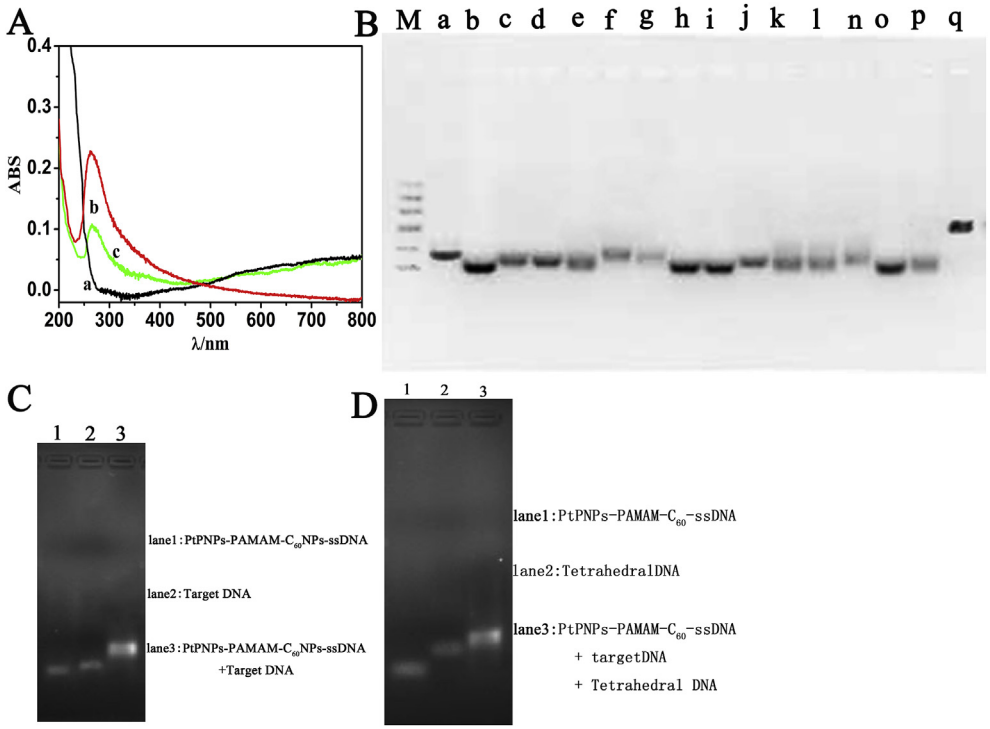

Fig. 3. (A) UV absorption spectra of (a) C_{60}NPs-PAMAM-PtPNPs, (b) ssDNA detection probe, and (c) C_{60}NPs-PAMAM-PtPNPs-ssDNA. (B) The SDS-PAGE image of the assembly of DNA tetrahedral. Lane q shows the DNA tetrahedral (S1+S2+S3+S4). Line a-d show the single-stranded DNA (S1, S2, S3, S4). Lines e-k show the two single-stranded DNA combinations (S1+S2, S1+S3, S1+S4, S2+S3, S2+S4, S3+S4). Lines l-p show the three single-stranded DNA combinations (S1+S2+S3, S1+S2+S4, S1+S3+S4, S2+S3+S4), respectively, and M (marker) is the 200-bp DNA ladder. (C) The SDS-PAGE image of (1) C_{60}NPs-PAMAM-PtPNPs-ssDNA, (2) target DNA and (3) the combination products of C_{60}NPs-PAMAM-PtPNPs-ssDNA and target DNA. (D) The SDS-PAGE image of (1) C_{60}NPs-PAMAM-PtPNPs-ssDNA, (2) tetrahedral DNA and (3) the combination products of C_{60}NPs-PAMAM-PtPNPs-ssDNA, target DNA and tetrahedral DNA.

3.3. Electrochemical behaviour of the DNA biosensor

The electrochemical characteristics of different nanomaterials were investigated. The results were mentioned in the supplement information (S2.1).

As shown in Fig. 4A, CV experiments were performed to monitor the modification procedure of the electrodes in a 5 mM $[Fe(CN)_6]^{3-/4-}$ solution. A pair of typical reversible redox peaks of ferricyanide ions can be observed on the bare GCE (curve a). After the electrode was modified with rGO-TEPA, the peak current of the CV increased (curve b), indicating the excellent electrical conductivity of rGO-TEPA. Meanwhile, from the results in Fig. S2D in the Supplementary information, we can see that the signal observed in rGO-TEPA (curve b) were higher than the bare GCE (curve a) and the net current increase significantly, which further proved that rGO-TEPA can indeed facilitate the electron transfer of the electrochemical biosensor. After AuNPs were electrodeposited on the above electrode, the peak current further increased (curve c), implying that AuNPs promote electron transfer. When the modified electrode was incubated with avidin (curve d), the peak current decreased due to the poor conductivity of avidin. When the modified electrode was immobilized with a biotinylated DNA tetrahedral probe (curve e), the peak current decreased due to the specific recognition between avidin and the biotinylated DNA tetrahedral probe, which hindered electron transfer. The peak current sharply declined after the biosensor was blocked with BSA (curve f) due to the formation of a hydrophobic protein layer.

EIS is one of the most powerful tools for probing the features of surface—modified electrodes [38]. Therefore, to further illustrate that all of the fabrication steps were effective, the electrochemical behaviours were characterized by electrochemical impedance spectroscopy using a 5 mM $[Fe(CN)_6]^{3-/4-}$ solution. It is well-known that the semicircle diameter in EIS is equal to the electron transfer resistance (R_{et}) and that the linear part of the curve at low frequency represents the diffusion process. As shown in Fig. 4B, when rGO-TEPA was modified onto the electrode, the resistance decreased (curve b) compared with the bare GCE (curve a), indicating that rGO-TEPA accelerated the electron transfer of the electrode. When AuNPs were electrodeposited onto the electrode, the resistance decreased (curve c), indicating that AuNPs promoted electron transfer between the electrode and the solution. Afterwards, a large semicircle diameter was observed when avidin was dropped onto the electrode (curve d), implying that avidin was successively immobilized onto the electrode. This larger diameter might be attributed to an insulating layer of proteins hindering the diffusion of electrons between the electrolyte and the electrode surface [39]. After the electrode was incubated with the biotinylated DNA tetrahedral probe (curve e), the R_{et} increased dramatically due to the nonconductive property of DNA. Subsequently, with BSA blocked onto the electrode, the resistance increased (curve f), indicating that the biosensor had indeed been successfully fabricated.

To highlight the advantages of the DNA tetrahedral probe in biosensors, we created two different types of capture probes, a DNA tetrahedral probe and ssDNA capture probe; these were also investigated by an EIS measurement. As shown in Fig. 4C, after the DNA tetrahedral probe was immobilized on the modified electrode, R_{et} increased (curve b) due to the negatively charged phosphate backbone of the DNA tetrahedral probe, which produces an electrostatic repulsion force to $[Fe(CN)_6]^{3-/4-}$. The semicircle was smaller compared with the ssDNA oligonucleotide capture probe modified electrode (curve c), indicating that the tetrahedral DNA

Please cite this article in press as: Y. Wan, et al., A novel DNA sensor based on C_{60}NPs-PAMAM-PtPNPs to detect VKORC1 gene for guiding rational clinical therapy with warfarin, Analytica Chimica Acta (2018), https://doi.org/10.1016/j.aca.2018.01.028

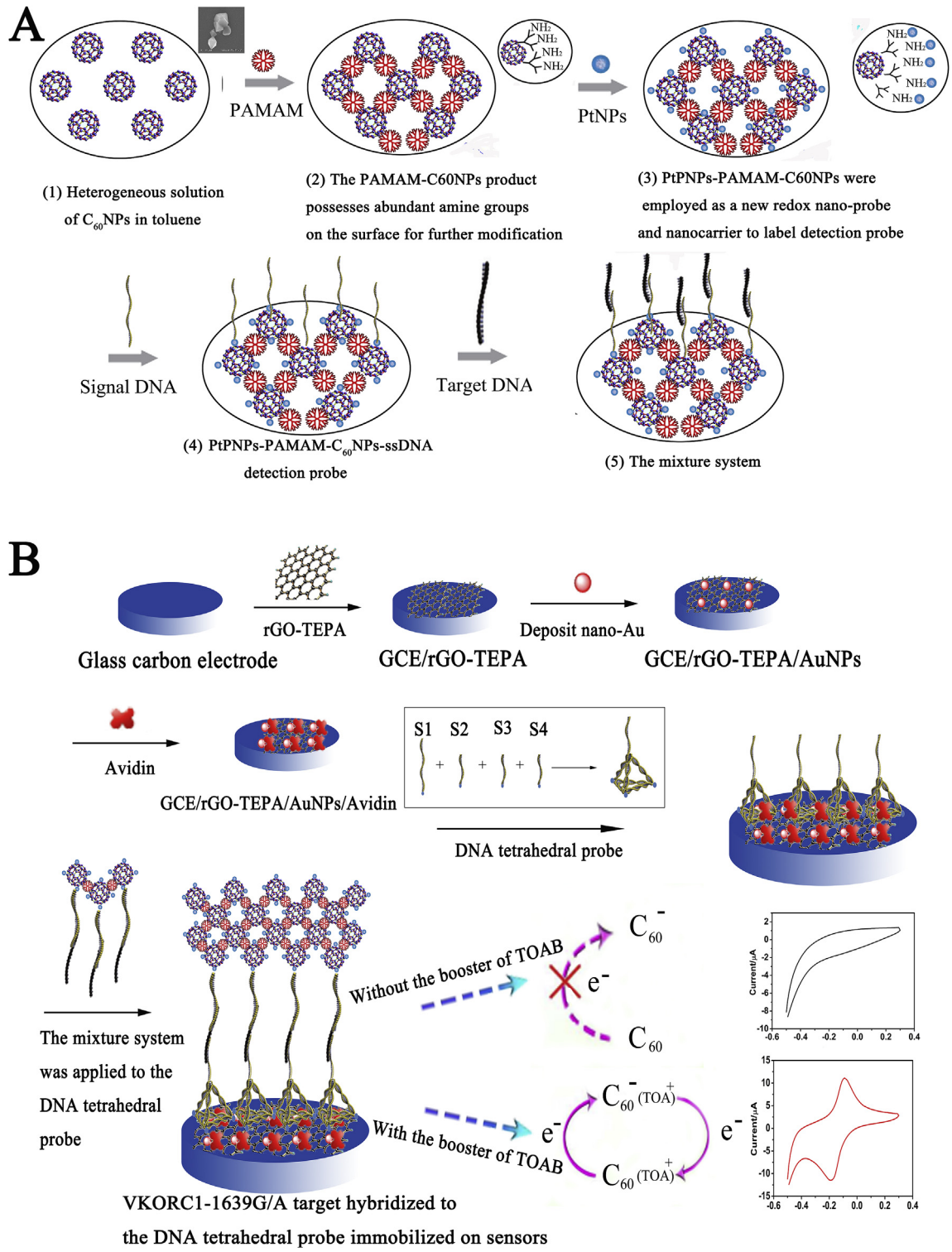

Scheme 1. (A) Preparation procedure of the detection probes. (B) Schematic illustration of the electrochemical DNA bioassay protocol.

nanostructure had relatively low resistance. Therefore, compared with the ssDNA probe, the DNA tetrahedral probe increased the detection signal.

To demonstrate the role of TOAB in C_{60}NPs-PAMAM-PtPNPs, CVs of different modified electrodes were detected in PBS (pH = 7.4). As shown in Fig. 4D, redox peaks were absence in the potential range from -0.5 to 0.3 V when the GCE/rGO-TEPA/AuNPs/avidin/DNA tetrahedral probe/BSA was incubated with target DNA and TOAB without the C_{60}NPs-PAMAM-PtPNPs-ssDNA detection probe (curve a) and when the GCE/rGO-TEPA/AuNPs/avidin/DNA tetrahedral probe/BSA was incubated with target DNA and the C_{60}NPs-PAMAM-PtPNPs-ssDNA detection probe without TOAB (curve b). When the GCE/rGO-TEPA/AuNPs/avidin/DNA tetrahedral probe/BSA was incubated with target DNA, C_{60}NPs-PAMAM-PtPNPs-

Please cite this article in press as: Y. Wan, et al., A novel DNA sensor based on C_{60}NPs-PAMAM-PtPNPs to detect VKORC1 gene for guiding rational clinical therapy with warfarin, Analytica Chimica Acta (2018), https://doi.org/10.1016/j.aca.2018.01.028

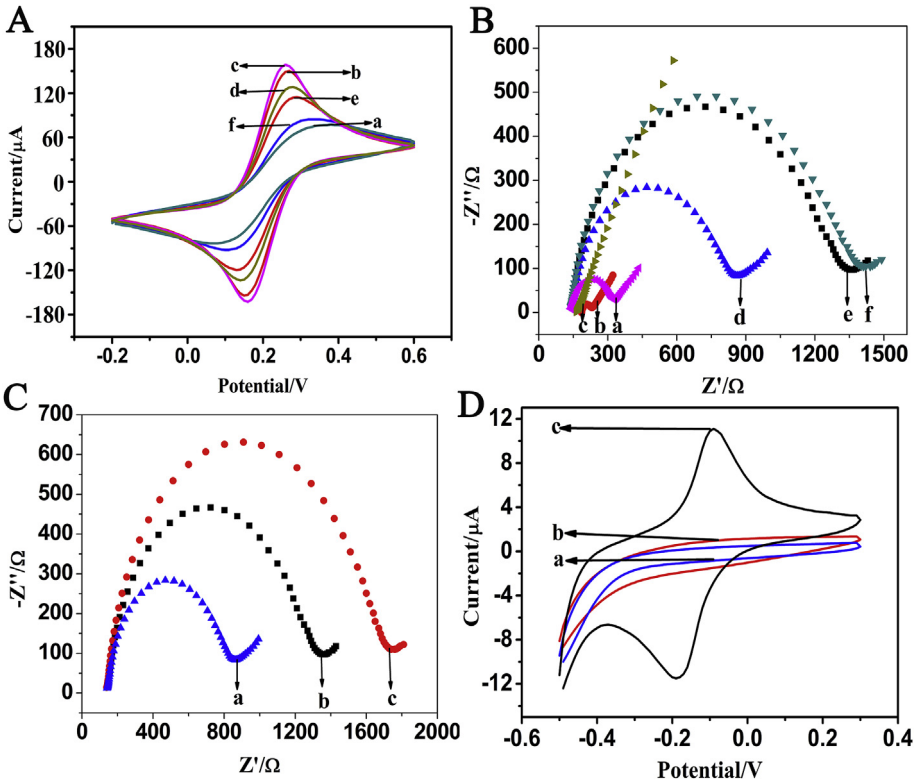

Fig. 4. (A) CV characterization of electrodes at various stages of modification in a 5 mM $[Fe(CN)_6]^{3-/4-}$ solution containing 0.1 M KCl: (a) bare GCE, (b) GCE/rGO-TEPA, (c) GCE/rGO-TEPA/AuNPs (d) GCE/rGO-TEPA/AuNPs/avidin, (e) GCE/rGO-TEPA/AuNPs/avidin/tetrahedral DNA, (f) GCE/rGO-TEPA/AuNPs/avidin/tetrahedral DNA/BSA; (B) EIS for each immobilization step in 5 mM $[Fe(CN)_6]^{3-/4-}$ containing a 0.1 M KCl solution: (a) bare GCE, (b) GCE/rGO-TEPA, (c) GCE/rGO-TEPA/AuNPs (d) GCE/rGO-TEPA/AuNPs/avidin, (e) GCE/rGO-TEPA/AuNPs/avidin/tetrahedral DNA, (f) GCE/rGO-TEPA/AuNPs/avidin/tetrahedral DNA/BSA in 5 mM $[Fe(CN)_6]^{3-/4-}$ containing a 0.1 M KCl solution. (C) The EIS spectra for the different modification steps: (a) GCE/rGO-TEPA/AuNPs/avidin; (b) GCE/rGO-TEPA/AuNPs/avidin/tetrahedral DNA; (c) GCE/rGO-TEPA/AuNPs/avidin/ssDNA in 5 mM $[Fe(CN)_6]^{3-/4-}$ containing a 0.1 M KCl solution. (D) CVs of different modified electrodes in 0.1 M PBS after incubation with 1 nM target VKORC1 followed by successive incubation with C_{60}NPs-PAMAM-PtPNPs-ssDNA and TOAB (c); incubation with C_{60}NPs-PAMAM-PtPNPs-ssDNA, but without TOAB (b); incubation with TOAB in the absence of the C_{60}NPs-PAMAM-PtPNPs-ssDNA bioconjugate (a).

ssDNA detection probe and TOAB, a pair of reversible redox peaks appeared (curve c); the anodic and cathodic peak potentials were −0.06 V and −0.15 V, respectively. This result demonstrated that TOAB acted as a booster to trigger the inner redox activity of the C_{60}NPs-PAMAM-PtPNPs, which is critical in the fabrication of biosensors.

3.4. Optimization of experimental conditions

The effects of the concentration of rGO-TEPA, deposition time of AuNPs, concentration of avidin, concentration of tetrahedral DNA, immobilization time of tetrahedral DNA and incubation time are discussed in detail in the Supplementary Information (S2.1). As a result, the following experiment were performed under the optimized conditions when the concentration of rGO-TEPA was 2.0 mg mL^{-1}, deposition time of AuNPs was 30 s, concentration of avidin was 100 ng mL^{-1}, concentration of tetrahedral DNA was 10 nM, immobilization time of tetrahedral DNA was 10 h and the incubation time was 60 min.

3.5. Analytical performance of the DNA biosensor

To evaluate the sensitivity and quantitative range of the developed DNA biosensor under the optimal assay conditions, the performance of the proposed biosensor was evaluated with different concentrations of target DNA. As indicated in Fig. 5A, the DPV peak currents increased with the increasing concentrations of target VKORC1 in the sample solution. The sample solution containing 3 mL of the serum sample was used for these experiments. In addition, as shown in Fig. 5B, the calibration curve showed good linear relationship between the DPV peak current changes (ΔI) and the logarithm values of the VKORC1 concentrations over the range of 1 pM−10 nM. The linear regression equation was $\Delta I\ (\mu A) = 2.332\ Lg\ C + 1.707$ (pM), with a correlation coefficient of 0.992. The comparison of the time consume between the proposed biosensors and other methods in literature was list in Table S3, which shows that the proposed method enabled faster detect efficiency of VKORC1. The detection limits were estimated to be 0.33 pM at a signal-to-noise ratio of 3σ (where σ is the standard deviation of the blank, n = 10). The proposed biosensor was also compared with other biosensor which used C_{60}. The results were shown that the biosensor in this study enable a wild liner range and lower detection limits in Table S4. The lower detection limits might be attributed to the presence of nanomaterials with excellent conductivity, which greatly amplifies the peak signals. The detection limits of the developed DNA biosensor can be used to detect VKORC1-1639 G/A in practical use.

3.6. Specificity, stability and reproducibility of the DNA biosensor

To investigate whether the biosensor could accurately interrogate a point-mutation, we challenged the biosensor with other oligonucleotides, such as single-base mismatch (mismatch-1, wild type), two-base mismatch (mismatch-2), three-base mismatch

Please cite this article in press as: Y. Wan, et al., A novel DNA sensor based on C_{60}NPs-PAMAM-PtPNPs to detect VKORC1 gene for guiding rational clinical therapy with warfarin, Analytica Chimica Acta (2018), https://doi.org/10.1016/j.aca.2018.01.028

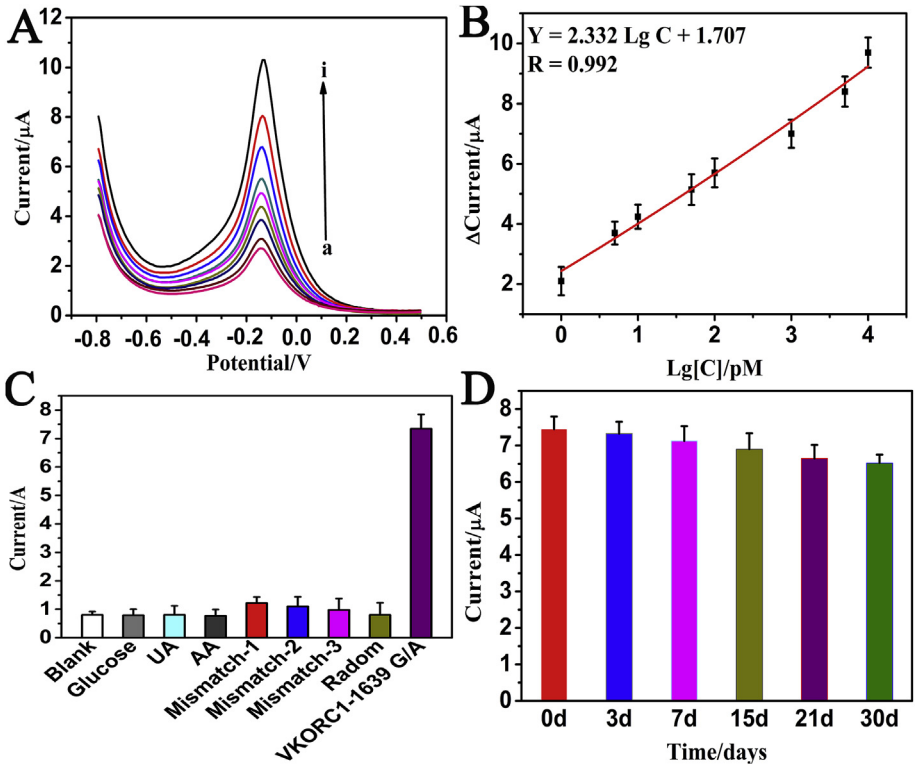

Fig. 5. (A) DPV signals of the DNA biosensor in the presence of different concentrations of VKORC1 and (B) the calibration curve of the DNA biosensor for different concentrations of VKORC1 (n = 3). (C) Specific response of the DNA biosensor spiked with blank, glucose, urea acid (UA) and ascorbic acid (AA) and after the biosensor was hybridized with mismatch-1(Wild type), mismatch-2, mismatch-3, a random sequence and complementary VKORC1 (1 nM for each analyse). (D) The stability of the VKORC1 DNA biosensor (1 nM) after 0 d, 3 d, 7d, 15 d, 21 d, and 30 d.

(mismatch-3) and non-complementary target (random). The responses of the biosensors were measured and are shown in Fig. 5C. Compared with the current response obtained from 1 nM VKORC1-1639 G/A, the responses caused by the mismatch sequences (1 nM for each one) were weak and negligible and were as low as the blank current. This indicated the high affinity of the biosensor to its complementary DNA target and that the developed biosensor could discriminate different DNA sequences effectively. The developed biosensor was used for the samples challenged with other related matrices, such as 50 mM glucose, 50 mM urea acid (UA) and 50 mM ascorbic acid (AA) (The concentrations of the above three interfering substances are far beyond those in normal serum.). A nearly negligible current change was obtained, which indicated that the developed biosensor could potentially be used in clinical application.

To evaluate the stability of the biosensor, we investigated long-term storage. The biosensor was stored at 4 °C when it was not in use and measured periodically. No obvious changes were observed during the first 3 days of storage, and the current changed by less than 1.6%. After 30 days of storage, it retained 87.49% of its initial response to 1 nM target (Fig. 5D). The comparison of stability with other reports was shown in Table S5. These results indicate the good stability of the proposed biosensor, which might be ascribed to the good biocompatibility of the C_{60}NPs-PAMAM-PtPNPs and rGO-TEPA.

To assess the reproducibility of the biosensor, the fabricated electrodes were assessed by intra- and interassay relative standard derivations (RSDs), as shown in Fig. S4 and Table S6 in the Supplementary Information. The intra-assay precision of the developed bioassay was calculated by detecting three samples containing 0.01, 1, and 10 nM of VKORC1. Each sample was measured five times using five biosensors prepared in parallel. For different concentrations of VKORC1, the intra-assay RSD values were less than 4.11%. The interassay precision was estimated by measuring one sample with three biosensors that were independently formed at the same GCE. As observed in Table S3, the RSD values were less than 4.09% for different concentrations of VKORC1. These results indicate that the proposed bioassay possesses acceptable precision and reproducibility.

3.7. Preliminary application of the DNA biosensor

The ultimate goal of developing a mutation-discriminating biosensor was to enable the direct analysis of mutated sequences in patient samples. Therefore, to test the potential application of the biosensor for practical analysis, the biosensor was used to test the recovery of three concentrations of VKORC1 in human serum samples, referencing the reported methods [11]. Three concentrations (1 pM, 0.1 nM and 10 nM) of VKORC1-spiked human serum samples were prepared by the standard addition method. The plasma samples were diluted to suitable concentrations with pH 7.4 PBS (1:10). It can be observed from Table S6 that the relative standard deviations were in the range of 1.90−3.33% and that the recoveries were in the range of 89.10−100.47%. These results show that the developed biosensor might be preliminarily applied to determine the presence of VKORC1 in real samples.

4. Conclusion

In summary, a novel DNA biosensor was successfully developed in an electrochemical bioassay of VKORC1 using C_{60}NPs-PAMAM-PtPNPs as a redox probe and avidin-coupled rGO-TEPA/AuNPs as a

Please cite this article in press as: Y. Wan, et al., A novel DNA sensor based on C_{60}NPs-PAMAM-PtPNPs to detect VKORC1 gene for guiding rational clinical therapy with warfarin, Analytica Chimica Acta (2018), https://doi.org/10.1016/j.aca.2018.01.028

substrate to immobilize a tetrahedral DNA capture probe. The proposed method has the following advantages: (1) C_{60}NPs-PAMAM-PtPNPs are used as a redox probe in a DNA biosensor for the first time and (2) a tetrahedral DNA capture probe is used for the recognition of target DNA, and the capture probes exhibit good orientation, controlled density at the biosensor interface, and enhanced biosensor sensitivity by controlling the biomolecule-confined surface to increase molecular recognition. Significantly, the universal method demonstrated here opens up a new approach for the determination of other relevant mutations occurring in other types of disease. Therefore, the presence of multiple mutations may be interrogated simultaneously, allowing for a more detailed clinical prognosis.

Acknowledgements

The research was financed by the Science and technology project of Sichuan provincial health and Family Planning Commission (No. 16PJ550).

Appendix A. Supplementary data

Supplementary data related to this article can be found at https://doi.org/10.1016/j.aca.2018.01.028.

References

[1] T. Aomori, et al., Rapid single-nucleotide polymorphism detection of cytochrome P450 (CYP2C9) and vitamin K epoxide reductase (VKORC1) genes for the warfarin dose adjustment by the SMart-amplification process version 2, Clin. Chem. 55 (2009) 804–812.
[2] M. Fuchshuber-Moraes, J.A. Perini, D. Rosskopf, G. Suarez-Kurtz, Exploring warfarin pharmacogenomics with the extreme-discordant-phenotype methodology: impact of FVII polymorphisms on stable anticoagulation with warfarin, Eur. J. Clin. Pharmacol. 65 (2009) 789–793.
[3] W.S. Hur, et al., Coagulation factor XIIIa is inactivated by plasmin, Blood 126 (2015) 2329–2337.
[4] C.R. King, et al., Performance of commercial platforms for rapid genotyping of polymorphisms affecting warfarin dose, Am. J. Clin. Pathol. 129 (2008) 876–883.
[5] A. Kwon, et al., Pharmacogenetic distribution of warfarin and its clinical significance in Korean patients during initial anticoagulation therapy, J. Thromb. Thrombolysis 32 (2011) 467–473.
[6] S.A. Scott, L. Edelmann, R. Kornreich, R.J. Desnick, Warfarin pharmacogenetics: CYP2C9 and VKORC1 genotypes predict different sensitivity and resistance frequencies in the Ashkenazi and Sephardi Jewish populations, Am. J. Hum. Genet. 82 (2008) 495–500.
[7] Y. Wen, et al., DNA nanostructure-based ultrasensitive electrochemical microRNA biosensor, Methods 64 (2013) 276–282.
[8] J. Das, et al., An electrochemical clamp assay for direct, rapid analysis of circulating nucleic acids in serum, Nat. Chem. 7 (2015) 569–575.
[9] S. Liu, W. Su, Z. Li, X. Ding, Electrochemical detection of lung cancer specific microRNAs using 3D DNA origami nanostructures, Biosens. Bioelectron. 71 (2015) 57–61.
[10] Y. Li, et al., Analysis of telomerase activity based on a spired DNA tetrahedron TS primer, Biosens. Bioelectron. 67 (2015) 364–369.
[11] L. Liu, et al., Ultrasensitive electrochemical detection of microRNA-21 combining layered nanostructure of oxidized single-walled carbon nanotubes and nanodiamonds by hybridization chain reaction, Biosens. Bioelectron. 70 (2015) 351–357.
[12] M. Lin, et al., Target-responsive, DNA nanostructure-based E-DNA sensor for microRNA analysis, Anal. Chem. 86 (2014) 2285–2288.
[13] H. Pei, et al., Regenerable electrochemical immunological sensing at DNA nanostructure-decorated gold surfaces, Chem. Commun. 47 (2011) 6254–6256.
[14] S.X. Chen, D.Y. Zhang, G. Seelig, Conditionally fluorescent molecular probes for detecting single base changes in double-stranded DNA, Nat. Chem. 5 (2013) 782–789.
[15] S. Dong, et al., Electrochemical DNA biosensor based on a tetrahedral nanostructure probe for the detection of avian influenza a (H7N9) virus, ACS Appl. Mater. Interfaces 7 (2015) 8834–8842.
[16] D. Zeng, et al., A novel ultrasensitive electrochemical DNA sensor based on double tetrahedral nanostructures, Biosens. Bioelectron. 71 (2015) 434–438.
[17] J. Zhang, Y. Yuan, S. biXie, Y. Chai, R. Yuan, Amplified amperometric aptasensor for selective detection of protein using catalase-functional DNA-PtNPs dendrimer as a synergetic signal amplification label, Biosens. Bioelectron. 60 (2014) 224–230.
[18] T. Hianik, M. Snejdarkova, M. Rehak, R. Krivanek, E. Meszar, J. Dujsík, I. Stepanek, D.P. Nikolelis, Binding of avidin modified antibody to biotinylated metal supported membranes and liposomes changes the physical properties of lipid bilayer, Gen. Physiol. Biophys. 17 (1998) 239–252.
[19] V. Ostatna, H. Vaisocherova, J. Homola, T. Hianik, Effect of the immobilisation of DNA aptamers on the detection of thrombin by means of surface plasmon resonance, Anal. Bioanal. Chem. 391 (2008) 1861–1869.
[20] A. Miodek, G. Castillo, T. Hianik, H. Korri-Youssoufi, Electrochemical aptasensor of human cellular prion based on multiwalled carbon nanotubes modified with dendrimers: a platform for connecting redox markers and aptamers, Anal. Chem. 85 (2013) 7704–7711.
[21] A. Guo, et al., An electrochemical immunosensor for ultrasensitive detection of carbohydrate antigen 199 based on Au@Cu(x)OS yolk-shell nanostructures with porous shells as labels, Biosens. Bioelectron. 63 (2015) 39–46.
[22] J. Han, Y. Zhuo, Y.Q. Chai, Y. Xiang, R. Yuan, New type of redox nanoprobe: C60-based nanomaterial and its application in electrochemical immunoassay for doping detection, Anal. Chem. 87 (2015) 1669–1675.
[23] A. Barberis, et al., Simultaneous amperometric detection of ascorbic acid and antioxidant capacity in orange, blueberry and kiwi juice, by a telemetric system coupled with a fullerene- or nanotubes-modified ascorbate subtractive biosensor, Biosens. Bioelectron. 67 (2015) 214–223.
[24] W. Zhilei, L. Zaijun, S. Xiulan, F. Yinjun, L. Junkang, Synergistic contributions of fullerene, ferrocene, chitosan and ionic liquid towards improved performance for a glucose sensor, Biosens. Bioelectron. 25 (2010) 1434–1438.
[25] Y.F. Gao, et al., Direct electrochemistry of glucose oxidase and glucose biosensing on a hydroxyl fullerenes modified glassy carbon electrode, Biosens. Bioelectron. 60 (2014) 30–34.
[26] Y. Cao, et al., Large-scale template-free synthesis of ordered mesoporous platinum nanocubes and their electrocatalytic properties, Nanoscale 7 (2015) 19461–19467.
[27] N. Liu, Z.F. Wang, Z.F. Ma, Platinum porous nanoparticles for the detection of cancer biomarkers: what are the advantages over existing techniques? Bioanalysis 6 (2014) 903–905.
[28] G. Hernandez-Cancel, D. Suazo-Davila, J. Medina-Guzman, M. Rosado-Gonzalez, L.M. Diaz-Vazquez, K. Griebenow, Chemically glycosylation improves the stability of an amperometric horseradish peroxidase biosensor, Anal. Chim. Acta 854 (2015) 129–139.
[29] P. Bollella, L. Gorton, R. Ludwig, R.A. Antiochia, Third generation glucose biosensor based on cellobiose dehydrogenase immobilized on a glassy carbon electrode decorated with electrodeposited gold nanoparticles: characterization and application in human saliva, Sensors 17 (2017) 1912–1924.
[30] Y. Li, et al., An electrochemical immunosensor for sensitive detection of Escherichia coli O157:H7 using C60 based biocompatible platform and enzyme functionalized Pt nanochains tracing tag, Biosens. Bioelectron. 49 (2013) 485–491.
[31] E. Kılınç, Fullerene C60functionalized γ-Fe2O3magnetic nanoparticle: synthesis, characterization, and biomedical applications, Artificial Cells, Nanomedicine, and Biotechnology 44 (2014) 298–304.
[32] T.H. Dung, L.T. Do, T.T. Loan, H. Yoo, Preparation and biophysical characterization of poly(amidoamine) dendrimer-poly(acrylic acid) graft, J. Nanosci. Nanotechnol. 15 (2015) 684–687.
[33] P. Chanphai, H.A. Tajmir-Riahi, Binding analysis of antioxidant polyphenols with PAMAM nanoparticles, J. Biomol. Struct. Dyn. 1 (2017) 28–36.
[34] P. Chanphai, H.A. Tajmir-Riahi, Trypsin and trypsin inhibitor bind PAMAM nanoparticles: effect of hydrophobicity on protein–polymer conjugation, J. Colloid Interface Sci. 461 (2016) 419–424.
[35] E. Froehlich, J.S. Mandeville, C.J. Jennings, R. Sedaghat-Herati, H.A. Tajmir-Riahi, Dendrimers bind human serum Albumin, J. Phys. Chem. B 113 (2009) 6986–6993.
[36] Y. Wang, Y. Zhang, T. Yan, D. Fan, B. Du, H. Ma, Q. Wei, Ultrasensitive electrochemical aptasensor for the detection of thrombin based on dual signal amplification strategy of Au@GS and DNA-CoPd NPs conjugates, Biosens. Bioelectron. 80 (2016) 640–646.
[37] G.J. Lia, L.H. Liu, X.W. Qia, Y.Q. Guo, W. Sun, X.L. Lia, Development of a sensitive electrochemical DNA sensor by 4-aminothiophenol self-assembled on electrodeposited nanogold electrode coupled with Au nanoparticles labeled reporter ssDNA, Electrochim. Acta 63 (2012) 312–317.
[38] G. Yuan, et al., A simultaneous electrochemical multianalyte immunoassay of high sensitivity C-reactive protein and soluble CD40 ligand based on reduced graphene oxide-tetraethylene pentamine that directly adsorb metal ions as labels, Biosens. Bioelectron. 72 (2015) 237–246.
[39] G. Yuan, H. Chen, C. Xia, L. Gao, C. Yu, Ultrasensitive electrochemical detection of secretoneurin based on Pb^{2+}-decorated reduced graphene oxide-tetraethylene pentamine as a label, Biosens. Bioelectron. 69 (2015) 95–99.

Please cite this article in press as: Y. Wan, et al., A novel DNA sensor based on C_{60}NPs-PAMAM-PtPNPs to detect VKORC1 gene for guiding rational clinical therapy with warfarin, Analytica Chimica Acta (2018), https://doi.org/10.1016/j.aca.2018.01.028